Active corrosion protection of various aluminium alloys by lithium-leaching coatings

Visser, Peter; Terryn, Herman; Mol, Johannes M.C.

DOI
10.1002/sia.6638

Publication date
2019

Document Version
Final published version

Published in
Surface and Interface Analysis

Received: 31 October 2018 | Revised: 18 February 2019 | Accepted: 20 February 2019

DOI: 10.1002/sia.6638

SPECIAL ISSUE ARTICLE

WILEY SURFACE and INTERFACE ANALYSIS

Active corrosion protection of various aluminium alloys by lithium-leaching coatings

Peter Visser[1,2] | Herman Terryn[1,3] | Johannes M.C. Mol[1]

[1] Department of Materials Science and Engineering, Delft University of Technology, Delft, The Netherlands

[2] AkzoNobel, Sassenheim, The Netherlands

[3] Vrije Universiteit Brussel, Research Group Electrochemical and Surface Engineering (SURF), Brussels, Belgium

Correspondence
P. Visser, Delft University of Technology, Department of Materials Science and Engineering, Mekelweg 2, 2628 CD, Delft, The Netherlands; AkzoNobel, Rijksstraatweg 31, 2171 AJ, Sassenheim, The Netherlands.
Email: p.visser-1@tudelft.nl

This study presents the active protective properties of lithium-leaching coatings for a range of aluminium alloys. Coatings with and without lithium carbonate as leachable inhibitor were applied on the aluminium alloys, artificially damaged and exposed to the neutral salt spray. A combined approach of scanning electron microscopy and electrochemical measurements revealed that the lithium carbonate leaching coating provided effective corrosion inhibition on AA2024, AA7075, AA5083, and AA6014 by the formation of a protective layer in the defect area and preventing local corrosion processes despite the different intrinsic electrochemical activity of the alloys.

KEYWORDS

aluminium, active corrosion protection, alloy, inhibitor, lithium

1 | INTRODUCTION

The corrosion resistance of aluminium alloys depends on the heterogeneous microstructure from the alloying additions and heat treatments. The nature, concentration, and distribution of second-phase intermetallic particles is a dominant factor controlling localized corrosion mechanisms and kinetics as the electrochemical characteristics of the particles may differ from those of the surrounding matrix, which can make the alloy susceptible to localized corrosion.[1,2] Intermetallic particles with a more noble potential relative to the alloy matrix can facilitate cathodic reactions and initiate localized corrosion in the surrounding alloy.[3] On the other hand, intermetallic particles can have a more anodic potential compared with the alloy matrix which can result in anodic activity (including dealloying) of the intermetallic particle when exposed to a corrosive environment.[4]

Prior to this work, lithium (Li) salts gained interest as corrosion inhibitor for aluminium alloys after Gui and Devine demonstrated the passivation of AA6061-T6 in alkaline Li-carbonate solutions.[5] Based on this observation, Buchheit et al continued and formulated an approach for a chemical conversion coating for aluminium alloys based on alkaline Li-carbonate solutions.[6] It was found that the corrosion inhibiting performance of these conversion layers depended on the type of aluminium alloy. In general, the performance of the layers followed the intrinsic corrosion resistance of the aluminium alloys: AA1100 > AA6061-T6 > AA7075-T6 > AA2024-T3.[6]

Recent studies have demonstrated that lithium-leaching coatings provide fast and effective corrosion protection on high strength aluminium alloy AA2024-T3 and are regarded as a promising environmental friendly alternative for chromate-based coatings for active corrosion protection.[7,8] It was demonstrated, when exposed to neutral salt spray (NSS) conditions, Li-salts were able to leach from the organic coating-matrix to form a corrosion protective layer on the exposed aluminium alloy in an artificial coating defect.[9,10] The formation of the layer involves a multistep mechanism of oxide thinning, anodic dissolution, and a competitive growth-dissolution process.[11] Further characterisation revealed that the protective layer comprises mainly aluminium, oxygen, and lithium and features a three-layered structure of a columnar outer layer, a porous middle layer, and a dense layer near the aluminium substrate.[9] Electrochemical analysis demonstrated that the corrosion protective properties could be attributed to the dense inner layer.[12]

All recent studies with lithium-salts as a leachable corrosion inhibitor were performed on AA2024-T3, and no other substrates were

evaluated as yet. This study presents the first investigation of the active corrosion protective properties of lithium-leaching coatings on other alloys than AA2024-T3 under NSS (ASTM B-117) conditions. A set of industrially relevant alloys with different local electrochemical activities was selected. The relative order of corrosion susceptibility of these alloys increases from AA6014-T4 > AA5083-H111 > AA2024-T3 > AA7075-T6.[13] Organic coatings with and without Li-carbonate as leachable inhibitor were applied on the aluminium alloys, and the samples were damaged with an artificial scribe and exposed to the NSS corrosion test (ASTM B-117). After the exposure, the samples were examined with an optical microscope, and a detailed investigation of the defect area was performed using scanning electron microscopy (SEM). Furthermore, the corrosion protective properties of the layers in the defect area were investigated using electrochemical impedance spectroscopy (EIS). The combination of these techniques provides a new insight into the corrosion protective properties of lithium-leaching coatings for these intrinsically different aluminium alloys.

2 | EXPERIMENTAL

2.1 | Materials and sample preparation

Aluminium alloys were acquired from various sources (Table 1).

The composition of the alloys and their major alloying elements (highlighted) are summarised in Table 2.[14]

Prior to the coating application, the panels were degreased with acetone to remove surface contaminations and abraded with Scotch-Brite 7447 PRO pads and finally cleaned again with acetone.

2.2 | Preparation of the organic model coatings

Epoxy-amine based model coatings were formulated, loaded with and without Li-carbonate as a leaching corrosion inhibitor. The formulations of the epoxy coatings are summarised in Table 3. The coating with Li-carbonate as leaching corrosion inhibitor contains 8 vol % pigment volume concentration (PVC) of Li-carbonate. Both coatings (with and without Li-carbonate) were formulated to a total PVC of 30 vol % using pigments and extenders.

The epoxy coatings were prepared according to the following procedure: the ingredients of Component A were added under stirring into a 370-ml glass jar. The pigments were dispersed to a fineness of grind less than 25 µm by shaking, on a Skandex paint shaker, using 400-grams Zirconox pearls (1.7-2.4 mm) as a grinding medium. The pearls were separated from the mixture after the dispersion phase. Component B was prepared separately and added to Component A prior to the application.

The coating formulations were spray applied on the abraded and cleaned alloys using a high-volume low-pressure (HVLP) spray gun. All samples were applied at ambient conditions at 23°C and 55% RH. After a 1-h flash-off period, the samples were cured in an oven (1 h at 80°C). The dry film thickness of the coatings was 28 ± 3 µm for all samples.

TABLE 3 Composition of organic model coatings

	Supplier	Without Inhibitor	Li-Carbonate
Component A			
Methyl isobutyl ketone	Brenntag	12.9 g	12.9 g
Epikote 828	Momentive	20.8 g	20.8 g
Lithium carbonate	Sigma Aldrich	-	6.9 g
Magnesium oxide	Sigma Aldrich	11.8 g	11.8 g
Tioxide TR 92	Huntsman	12.0 g	12.0 g
Blanc fixe N (Ba (SO_4))	Sachtleben	28.0 g	13.0 g
Component B			
Xylene	Brenntag	6.0 g	6.0 g
Ancamine 2500	Evonik	14.5 g	14.5 g
Dynasilan Glymo	Evonik	2.0 g	2.0 g

TABLE 1 Alloys used in this study and their intended application areas[33]

Alloy	Temper	Thickness	Supplier	Application Area
2024	T3	0.8 mm	Arconic	Aerospace
5083	H111	1.0 mm	Thyssen-Krupp	Automotive/marine
6014	T4	1.0 mm	Chemetall	Automotive
7075	T6	0.8 mm	Thyssen-Krupp	Aerospace/automotive

TABLE 2 Chemical composition of the aluminium alloys[14]

Alloy	Si	Fe	Cu	Mn	Mg	Cr	Zn	Ti	Others	Al
2024-T3	0.5	0.5	3.8–4.9	0.3-0.9	1.2-1.8	0.1	0.25	0.15	0.15	Rest
7075-T6	0.4	0.5	1.2-2.0	0.3	2.1-2.9	0.18-0.28	5.1-6.1	0.2	0.15	Rest
5083-H111	0.4	0.4	0.1	0.4-1.0	4.0-4.9	0.05-0.25	0.25	0.15	0.15	Rest
6014-T4	0.3-0.6	0.35	0.25	0.05-0.2	0.4-0.8	0.2	0.1	0.1	0.15	Rest

2.3 | Referencing of the samples

In this paper, the alloys that were coated with the Li-carbonate loaded coating will be referenced as AAXXXXW (eg, AA2024W), and the samples that were coated with the coating without Li-carbonate will be referenced as AAXXXXWO (eg, AA7075WO).

2.4 | Active corrosion protection in the defect area

The coatings were artificially damaged in order to assess the active protective properties of the lithium-leaching coating. On a sample panel of 7 × 7 cm, two intersecting scribes penetrating through the coating and 100 to 150 μm into the alloy with a width of 1 mm and a length of 2 cm were prepared by mechanical milling resulting in a defect with a surface area of 0.48 cm^2. The damaged samples were exposed to the NSS test according to ASTM-B117 for 168 hours. After the exposure, the defect areas were assessed for their appearance using optical microscopy. In addition, further assessments of the defect areas were performed using scanning electron microscopy and EIS.

2.5 | Scanning electron microscopy (SEM)

A JEOL JSM-7100F field emission SEM was used to investigate the defect areas. The surface morphology of the defect areas was examined in planar view with a lower electron detector (LED) at 5 kV and a working distance of 10 mm. Cross sections of the defect areas were prepared by polishing using a Hitachi IM4000 ion milling system at 6-kV Ar-ion acceleration, applying a 3 times-per-minute sample rotation speed and a swing angle of +/− 30°. These cross sections were examined using the backscatter electron detector (BED-C) at 5 kV and a working distance of 4 mm.

2.6 | Electrochemical assessment of the defect area

All electrochemical measurements were executed with a Gamry Interface 1000 computer-controlled potentiostat using an electrochemical cell with a three-electrode setup in a Faraday cage. The three-electrode setup consisted of a saturated calomel electrode (SCE) as reference electrode, the coating defect area as the working electrode, and a graphite counter electrode. The electrochemical cell had a total surface area of 12.5 cm^2, and the effective electrode (ie, the coating defect) area was 0.48 cm^2.

Potentiodynamic polarisations were performed in a 3.5% NaCl solution to obtain comparative information related to the electrochemical activity in terms of kinetics of anodic and cathodic reactions in the defect areas of the different aluminium alloys. In order to assess the electrochemical behaviour in the defect area of the different alloys under potentiodynamic polarisation conditions, the aluminium panels were masked with a polyester tape and mechanically milled as described above for the coatings. The open circuit potential (OCP) was measured for 10 minutes prior to polarisation to establish an approximately stable potential. It was found that 10 minutes was sufficient time for the OCP to stabilise in the defect area to obtain reproducible potentiodynamic polarisation measurements. The samples were polarised using a sweep rate of 0.5 mV/s and a sweep range of −300 and +300 mV versus the OCP. Separate samples were used for anodic and cathodic potentiodynamic polarisations starting from the OCP. In order to assess reproducibility, all tests were performed in triplicate for each anodic and cathodic polarisation. The polarisation curves were used to approximate the corrosion current density (i_{corr}) of the alloys from the linear slope of the linear region ±20 mV vs. E_{corr} using the Stern-Geary equation.[15,16]

Electrochemical impedance spectroscopy (EIS) was applied to assess the corrosion activity and inhibition in the defect area with a surface area of 0.48 cm^2 before and after exposure to the NSS test. The EIS measurements were performed at the OCP in a 0.05 M NaCl solution as electrolyte over a frequency range from 10^{-2} to $2{\cdot}10^4$ Hz, applying a 10-mV sinusoidal amplitude and recording 10 measurements per frequency decade. The impedance spectra were fitted with Zview from Scribner Associates Inc. using the appropriate equivalent circuits (ECs) for further data analysis. The values resulting from the fitting were scaled to a surface area of 1 cm^2.

3 | RESULTS AND DISCUSSION

3.1 | Optical observations of the scribed defect areas after NSS exposure

The defect areas of the coated alloys were examined with an optical microscope after 168-hour exposure to NSS. The optical images, displayed in Figure 1, show the effects of the corrosive conditions in the scribed areas after exposure to the NSS of the coated alloys with and without Li-carbonate as leaching inhibitor. The detrimental effects of these corrosive conditions are observed on the samples coated with the coating without an inhibitor. Especially the samples of AA2024WO and AA7075WO (Figure $1A_{(wo)}$ and $1B_{(wo)}$) show a darkened scribe with a significant amount of voluminous corrosion products and extensive corrosion creeping under the coating from the defect area. Apart from some darkening of the scribed area, the other alloys, AA5083WO, and AA6014WO (Figure $1C_{(wo)}$ and $1D_{(wo)}$) do not show severe signs of corrosion nor extensive corrosion underneath the coatings. The corrosion inhibiting effect of the coatings loaded with Li-carbonate as leachable corrosion inhibitor on the different alloys can clearly be observed from the corresponding images (Figure $1A_{(w)}$-$1D_{(w)}$). All alloys coated with the lithium-loaded coatings show almost pristine scribes without corrosion products and no corrosion creep under the coating.

3.2 | Detailed morphological observations in the scribed defect area after NSS exposure

The defect areas were examined in more detail using SEM. Figure 2 shows top-view SEM micrographs of the scribed area of the samples discussed in the previous section. This figure shows the large amount of corrosion products in the scribed areas of AA2024WO and AA7075WO (Figure $2A_{wo}$ and $2B_{wo}$) after the NSS exposure when the coating did not contain Li-carbonate as leachable corrosion inhibitor.

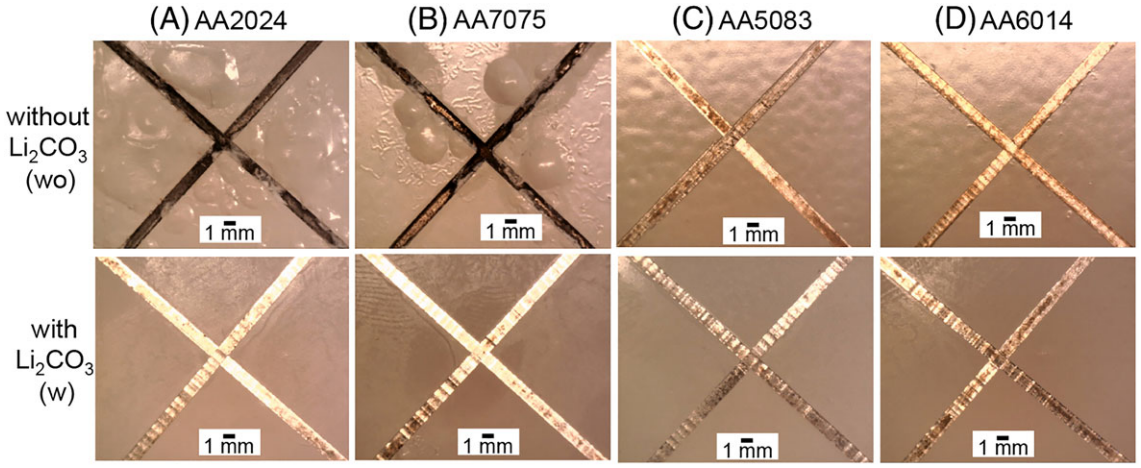

FIGURE 1 Optical images of the coated and scribed panels of the different aluminium alloys after 168-h neutral salt spray exposure (ASTM B-117): A, AA2024-T3; B, AA7075-T6; C, AA5083-H111; and D, AA6014-T4 (WO) coating without and (W) with Li-carbonate

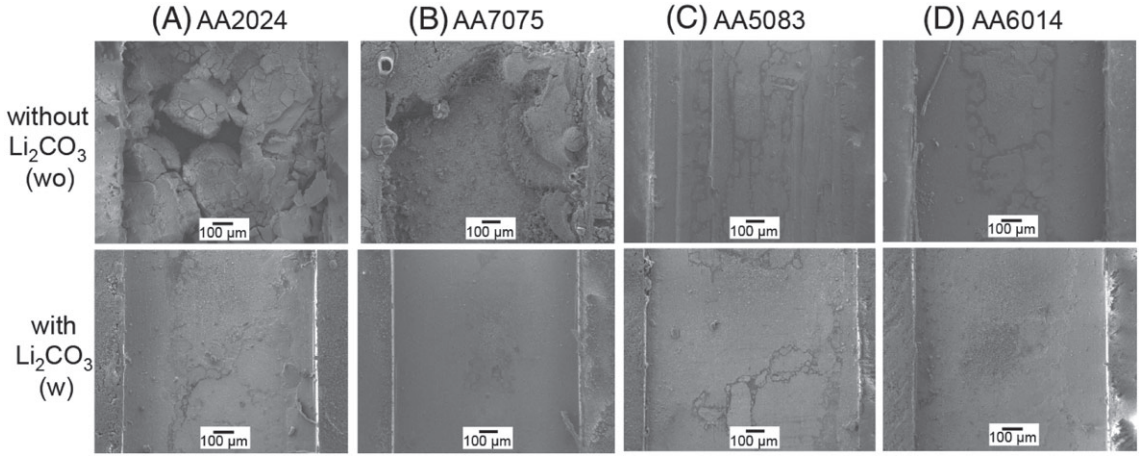

FIGURE 2 SEM micrographs of the top-view appearance of the scribes of the samples after 168-h neutral salt spray exposure (ASTM B-117): A, AA2024-T3; B, AA7075-T6; C, AA5083-H111; and D, AA6014-T4, (WO) coating without and (W) with Li-carbonate

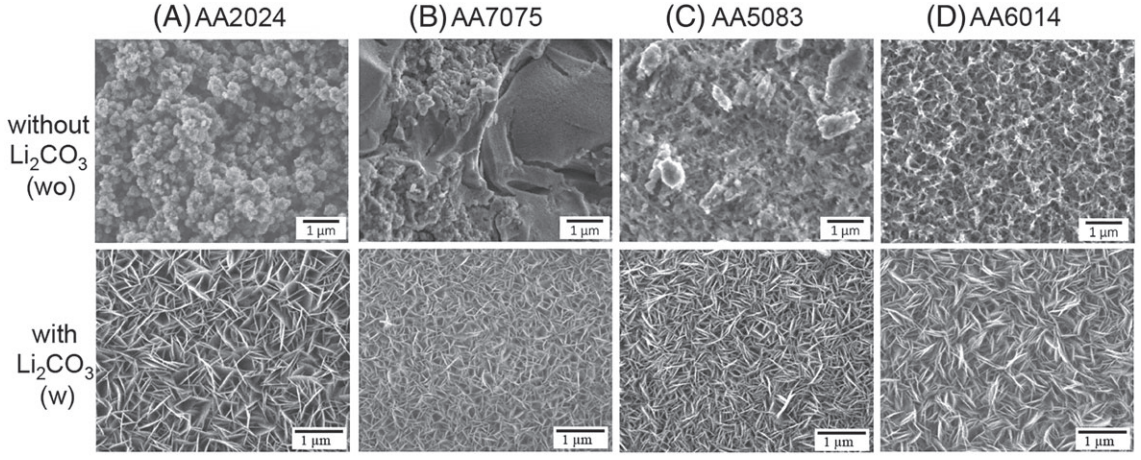

FIGURE 3 SEM micrographs of the top-view morphology of the layer in the scribe after 168-h neutral salt spray exposure (ASTM B-117): A, AA2024-T3; B, AA7075-T6; C, AA5083-H111; and D, AA6014-T4, (WO) coating without and (W) with Li-carbonate

The corresponding images of these alloys (Figure $2A_w$ and $2B_w$) show the corrosion inhibiting effect on these alloys of the Li-carbonate loaded coatings, clearly revealing scribes without any signs of corrosion in the defect area. The micrographs of the other alloys (AA5083 and AA6014) show no significant differences between the samples with and without Li-carbonate. It can be observed that all scribes are covered with a layer, but no severe corrosion was observed at this magnification.

Figure 3 shows a more detailed overview of the surface morphologies of a representative area of each of the scribes at higher magnification. It shows a clear difference in the surface morphology of the layers in the defect areas of the samples without Li-carbonate (Figure $3A_{wo}$-$3D_{wo}$) compared with the samples with the Li-carbonate loaded coating (Figure $3A_w$-$3D_w$). Figure $3A_{wo}$ and $3B_{wo}$ shows the voluminous corrosion products present in the scribes of AA2024WO and AA7075WO. The scribe of AA5083WO did not show a lot of corrosion products with the optical and initial SEM assessment of the scribed area, but the magnified micrograph (Figure $3C_{wo}$) shows a layer of dense corrosion products. Figure $3D_{wo}$ reveals that the scribe of AA6014WO is covered with a layer with the morphology of a hydrated aluminium oxide, which can indicate that the substrate is affected by corrosion. In contrast to these samples, all the scribes of the alloy samples coated with the Li-carbonate loaded coatings were covered by a layer with a polycrystalline morphology, featuring intersecting plate-like crystals that is commonly observed for layered double hydroxide compounds generated on aluminium[6,17,18] and is typical for the protective layer generated from the lithium-leaching coating technology.[9,19] The size of the crystals varies per alloy, but it is evident that the formation of these layers is a result from the active protective nature of the lithium-leaching coatings.

3.3 | Cross-sectional analysis of the defect areas after NSS exposure

Ion-milled cross sections of the defect areas were prepared to study these layers and the effects of the NSS exposure on the different alloys in more detail using SEM. Figure 4 shows the cross-sectional micrographs of the defect areas of the alloys after 168-hour NSS exposure. Figure $4A_{wo}$ shows the cross section of the corroded surface of the scribe of the AA2024WO sample. The layer of corrosion products is about 6 μm thick and has been formed due to the detrimental effects of the corrosive environment during the NSS exposure. The alloy surface is severely attacked. In contrast to this, a layer of 2-μm thickness is formed on the AA2024W sample (Figure $4A_w$). The layer has the characteristic three-layered morphology, featuring a dense inner layer, a porous middle layer, and a columnar outer layer as observed in previous work on AA2024-T3, and no signs of (local) corrosion phenomena were observed.[9]

The defect area of the AA7075WO sample (Figure $4b_{wo}$) shows severe corrosion into the substrate besides a layer of voluminous corrosion products, with a thickness of more than 10 μm. Similar to AA2024W, a layer with the three-layered morphology, with an approximate thickness of 1.0 μm, was formed on the aluminium substrate in the defect of the AA7075W sample (Figure $4B_w$). The cross-sectional analysis of the defect area of the sample AA5083WO (Figure $4C_{wo}$) shows no significant amounts of corrosion products after 168-hour NSS exposure. A thin oxide layer is present on the aluminium surface in the defect, and the alloy seems to be locally affected by corrosion of specific grains at the surface of the scribe, possibly due to local anodic dissolution of magnesium. However, such local corrosion attacks were not observed in the defect areas of the AA5083W sample. Similar to AA2024W and AA7075W, a protective layer with a typical three-layered morphology with a total thickness of 1.5 to 2 μm was formed in the defect area after the NSS exposure (Figure $4C_w$). A similar protective layer was formed in the defect area of the sample of the AA6014W sample after 168-h NSS exposure (Figure $4D_w$) Whereas optically, the defect of the AA6014WO sample looked optically still free of corrosion, the cross-sectional analysis revealed (intergranular) corrosion of the substrate (Figure $4D_{wo}$). These observations show that a layer is formed in the defect areas of all alloys when a Li-leaching coating was used independent from the alloy composition. Despite some slight differences in contrast and thickness, in general, the layers feature the similar characteristic

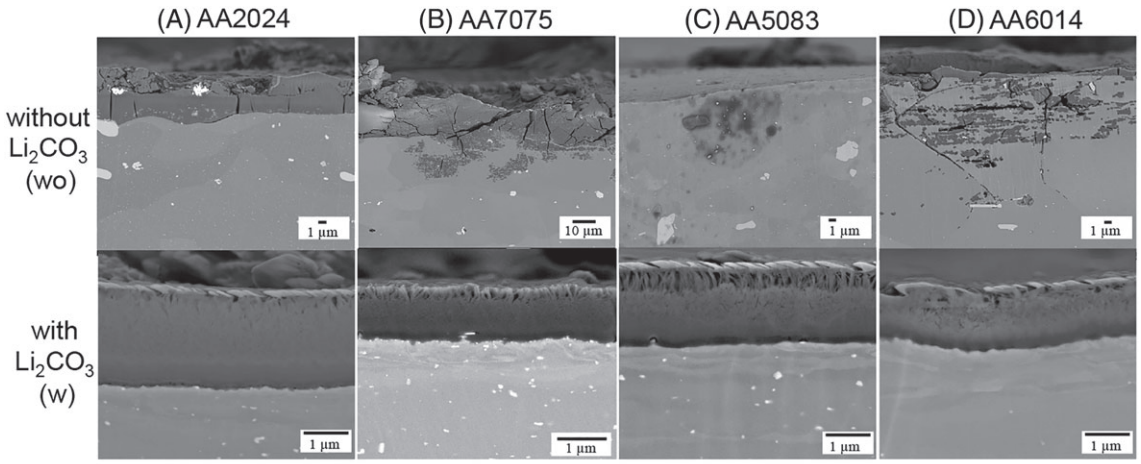

FIGURE 4 Cross-sectional scanning electron micrographs of the scribes of the different alloys after 168-h NSS exposure (ASTM B-117): A, AA2024-T3; B, AA7075-T6; C, AA5083-H111; and D, AA6014-T4 (WO) coating without and (W) with Li-carbonate

morphology of a dense inner layer, a porous middle layer, and columnar outer layer known for protective layers generated from Li-leaching coatings Furthermore, the results confirm that AA5083-H111 and AA6014-T4 are less sensitive to corrosion compared with the 2XXX and 7XXX series of alloys.[20]

3.4 | Corrosion protective properties the layers in the defect areas of the different alloys

3.4.1 | Electrochemical activity of the defect areas prior to exposure

Potentiodynamic polarisation measurements were performed on the taped panels with a scribed defect area to determine the difference of the electrochemical activity in the defect areas of the different alloys. Figure 5 shows the potentiodynamic polarisation curves recorded for each of the alloys. When polarised anodically, AA6014-T4 and AA5083-H111 show a passive range and a distinct pitting potential (E_{pit}), whereas, the high strength aluminium alloys (AA2024-T3 and AA7075-T6) show their typical active character.[21,22] Furthermore, the alloys show different cathodic reaction kinetics. The values of corrosion potential (E_{corr}), pitting potential (E_{pit}), and the corrosion current density (i_{corr}) were derived from the potentiodynamic polarisation curves and summarised in Table 4.

The high-strength aluminium alloys, AA2024-T3 and AA7075-T6, have a more noble E_{corr} compared with AA6014-T4 and AA5083-H111. In addition, it can be observed that the cathodic branches of these alloys have higher current density values indicating faster cathodic reaction kinetics. The magnitude of this E_{corr} shift and increased cathodic reaction kinetics is related to the copper content in the alloy.[13] The low copper alloys (AA6014-T4 and AA5083-H111) show a reproducible and similar E_{pit} but differ slightly in E_{corr} and cathodic reaction kinetics (AA6014-T4 < AA5083-H111). For AA7075-T6 with a copper content of (1.2-2 wt.%), the E_{corr} shifts

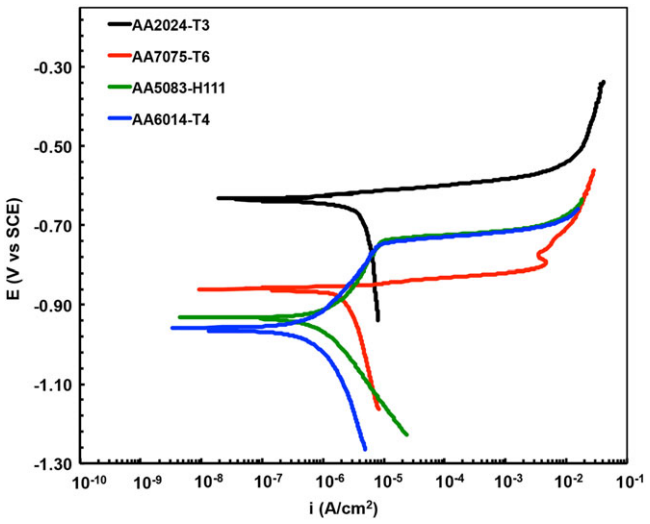

FIGURE 5 Potentiodynamic polarisation curves of the damaged areas of aluminium alloys in 3.5% NaCl solution

TABLE 4 Electrochemical parameters obtained from the potentiodynamic polarisation curves of the different alloys displayed in Figure 5

	Ecorr (V_{SCE})	i_{corr} ($\mu A/cm^2$)	Passive Range E_{pit}-E_{corr} (V)
2024-T3	−0.638 ± 0.01	4.4 ± 1.7	0
7075-T6	−0.859 ± 0.01	5.0 ± 0.2	0
5083-H111	−0.927 ± 0.01	1.5 ± 0.1	0.2 ± 0.01
6014-T4	−0.957 ± 0.02	1.4 ± 0.0	0.23 ± 0.02

68 mV to the more noble potentials and higher cathodic reaction kinetics. AA2024-T3 shows an even larger shift to more noble potential (289 mV) due to the higher copper content (3.8-4.9 wt. % Cu); also, here an increase in the cathodic reaction kinetics is observed. All together, this leads to significant higher corrosion current density values compared with the low copper alloys. Considering these observations and the i_{corr} values of 5.0 and 4.4 $\mu A/cm^2$ for, respectively, AA7075-T6 and AA2024-T3 compared with the i_{corr} values of 1.5 and 1.4 $\mu A/cm^2$ for AA5083-H111 and AA6014-T4, the defect areas of the aluminium alloys can be ordered based on increasing electrochemical activity or corrosion sensitivity: AA6014-T4 < AA5083 < < AA2024-T3 < AA7075-T6.

3.4.2 | EIS measurements

EIS was used to measure the electrochemical characteristics of the layers formed in the defects of the different alloys from the coatings with and without Li-carbonate. Figure 6 shows the recorded EIS spectra of the coated alloys before and after the 168-hour NSS exposure. The figure shows the Bode plots of the impedance modulus and the accompanying phase angle plots of the measurements for each alloy. Each graph shows a measurement of an unexposed sample to demonstrate the initial stage of the defect area with the native aluminium oxide and the measurements of the samples with and without Li-carbonate after 168-hour NSS exposure. Figure 6A shows the typical response of the impedance modulus (top) and phase angle (bottom) of a AA2024-T3 coated with and without Li-carbonate as leaching inhibitor.[12] The impedance modulus (Figure $6A_{top}$) of the sample with the Li-carbonate loaded coating increased in the middle (10^1-10^3 Hz) and low frequency (10^{-1}-10^{-2} Hz) ranges compared with the samples without Li-carbonate and the unexposed sample. This increase of the impedance modulus can be attributed to the formation of an oxide layer and the increased corrosion resistance of such layers in the defect area.[23,24] Figure $6A_{bottom}$ shows the phase angle diagrams of the respective AA2024-T3 samples. The phase angle plot of the unexposed sample shows two time-constants, one at 10^1 Hz associated with the native oxide layer and one time-constant around $2{\cdot}10^{-2}$ Hz for the electrochemical activity at the aluminium substrate in the coating defect.[25] Compared with the unexposed sample and the sample without Li-carbonate, the phase angle plot of the sample with the Li-carbonate loaded coating showed a

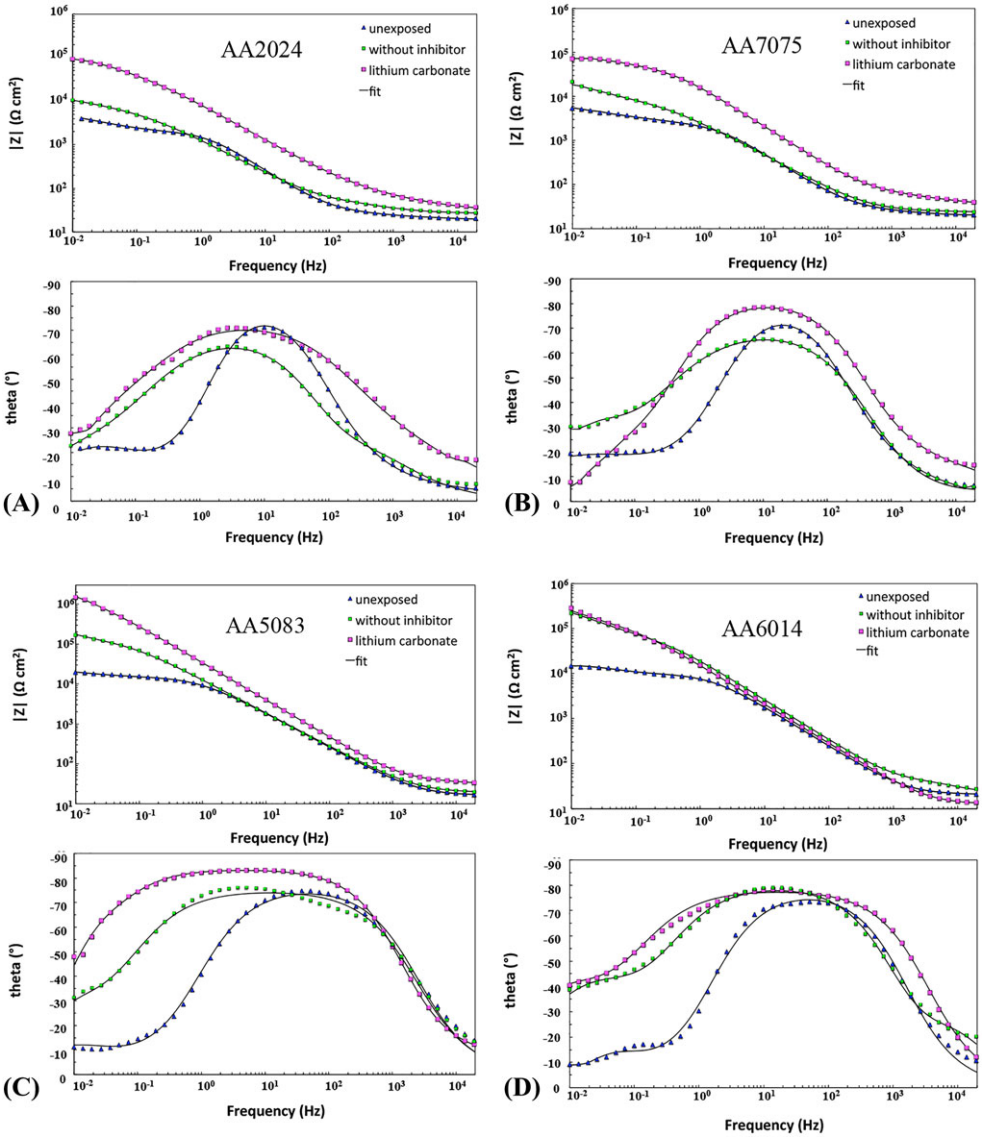

FIGURE 6 Electrochemical impedance spectra of the coated aluminium alloys with a defect area in 0.05 M NaCl solution before and after 168-h NSS. A, AA2024; B, AA7075; C, AA5083; and D, AA6014 showing impedance modulus (top) and phase angle plots (bottom)

broadening of the time-constant related with formation of the oxide layer and increases phase angle values at the lower frequency range which indicates improved corrosion resistance. This behaviour is characteristic for the Li-leaching coating technology on AA2024-T3.[12,19] A similar behaviour was observed for the samples with the Li-carbonate loaded coatings on the AA7075W (Figure 6B) and the AA5083W (Figure 6C) after 168-hour NSS exposure. Therefore, it can be stated that the generated layers in the defects of these alloys provide enhanced corrosion protective properties. The sample with the Li-carbonate loaded coating on AA6014 showed a slightly different behaviour (Figure 6D). Whereas, the cross section revealed the formation of a protective layer in the defect of the AA6014 aluminium alloy, the impedance modulus in the middle frequency range does not increase significantly for the AA6014W sample. However, the low frequency impedance increased about 10 times for both the samples AA6014WO and AA6014W compared with the unexposed sample. While initially the differences in the Bode magnitude plot are relatively small, it is clear from the cross-sectional analysis that the layer generated in the defect area of AA6014W provided additional corrosion protection compared with the sample AA6014WO.

3.4.3 | Electrochemical properties of the protective layers

Three physical models (Figure 7) were defined with their respective EC to fit the measurements and quantitatively describe the electrochemical properties of the layers present in the defect areas after the NSS exposure. The selection of the relevant ECs used for the fitting of the different samples was based on the physical morphology observed by the cross-sectional analysis of the defect area. EC1 is a model with two time-constants used to describe the effect in a defect area of a

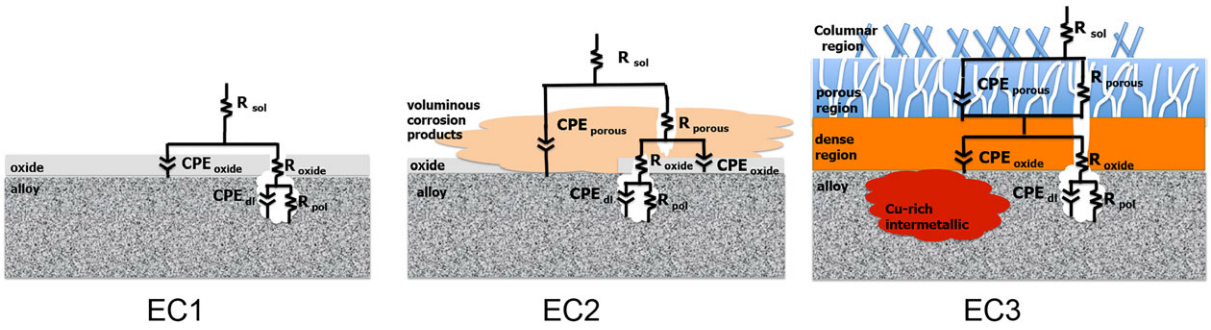

FIGURE 7 Equivalent electric circuits used to fit the EIS spectra: (EC1) unexposed defect areas and defect areas with few or no corrosion products; (EC2) defect areas with voluminous porous corrosion products; (EC3) defect areas with protective layer generated from the Li-carbonate loaded coatings

damaged coating representing the aluminium substrate with a thin or native oxide layer. In this EC, R_{sol} is the electrolyte resistance; R_{oxide} is the resistance of the (native) oxide layer, and the CPE_{oxide} is the constant phase element (CPE) describing the capacitance of the oxide layer using parameters Q_{oxide} and n_{oxide}. The electrochemical processes at the aluminium substrate are described in the second time-constant, by R_{pol} and CPE_{dl}, which represents the polarisation resistance and the double layer capacitance. The CPEs are used in these ECs to describe the frequency dependence of elements with a non-ideal capacitive behaviour and because of the nonuniformity of the generated layers in the defect.[26,27] EC 2 describes the physical model with an additional time-constant to account for the voluminous porous corrosion products (CPE_{porous} and R_{porous}) in the defect, on top of the oxide layer, and EC3 is the model that is used to describe the three-layered morphology of the protective layer that is generated from the Li-carbonate loaded coating.[12] The three time-constants of EC3 are represented by the following: R_{sol} for the electrolyte resistance, CPE_{porous} and R_{porous} and describe the contribution of the porous middle layer which is usually very minor, the dense inner layer at the aluminium substrate is represented by R_{oxide} and CPE_{oxide}, and the double layer capacitance and polarisation resistance at the metal/oxide interface are described by CPE_{dl} and R_{pol}. The fitted curves are displayed as solid lines in the Bode plots of Figure 6. The numerical values of the fittings from these spectra are listed in Table 5.

In order to compare the electrochemical properties of the defect areas, the equivalent capacitance of the oxide layer (C_{oxide}) and double layer (Cdl) in the different EC's was calculated using the respective CPE parameters (Q and n) and the resistance corresponding to each time-constant of the measurements summarised in Table 5 using the equation of to Hirschorn et al[28]:

$$C = R^{\frac{(1-n)}{n}} Q^{\frac{1}{n}}. \quad (1)$$

The results in Table 5 also show that there is a small contribution of the porous regions of the layers in the defects after 168-hour NSS exposure. The values of Q (CPE_{porous}) and R_{porous} mentioned in Table 5 represent the contribution of two different porous materials. In case of the coatings without lithium, this parameter represents the contribution of the voluminous corrosion products (EC2), and for the samples with lithium, it represents the contribution of the porous region in the protective layer. (EC3) The n values of $Q_{(CPE\ porous)}$ are around 0.5. This indicates that the contribution of the porous element does not behave as an ideal capacitor. These low n (CPE) values suggest a diffusion process or a porous electrode.[29] It is known that the protective layer in the defect area is not uniform, and capacitive values may vary throughout the layer. The relative contribution of the porous element of the layer is small and may seem insignificant compared with the parameters of the dense oxide layer. However, the physiochemical model used for the electrochemical analysis can be justified by the micrographs of the protective layers, and the contribution of the porous layer cannot be ignored for the fitting of the EC.[12]

Figure 8 shows the trends of the resistance and capacitance values of the oxide layer (R_{oxide} and C_{oxide}) and the metal/oxide interface (R_{pol} and C_{dl}) in the defects of different coated alloys before and after exposure to the NSS test. Figure 8A shows the corrosion inhibiting effect of the protective layer generated in the defect area on AA2024W after the NSS exposure. From the graph, it can be observed that both the resistance values (R_{oxide} and R_{pol}) of the sample AA2024W are 8 to 10 times higher compared with the sample AA2024WO or the unexposed sample. For the same sample, the capacitance values dropped to 32 and 320 μF/cm ^{2} for, respectively, C_{oxide} and C_{dl} which is in good agreement with previous findings.[12] These increased resistances and decreased capacitances are consistent with the presence of a corrosion protective layer in the defect area. Besides the optical and microscopy analysis, the EIS measurements demonstrate the weak corrosion resistance in the defect area of the sample AA2024WO. The R_{oxide} and R_{pol} remained low around 7 kΩ.cm^2, and the capacitance values increased to 180 and 1240 μF/cm^2 indicating the occurrence of corrosion. A similar behaviour as the AA2024 alloy is observed for the AA7075 and AA5083 alloys in Figure 8B and C. Both alloys show the increased resistances and strongly reduced capacitance values for the samples coated with the Li-carbonate loaded coating. These results clearly demonstrate that the layer in the defect area generated from the Li-carbonate

TABLE 5 Fitted parameters of the EIS spectra of the scribed coatings on the different aluminium alloys

AA2024-T3					AA7075-T6				
EC		Unexposed 1	Without inhibitor 2	Lithium leaching 3	EC		Unexposed 1	Without inhibitor 2	Lithium leaching 3
R_{sol}	Ω	24	24	28	R_{sol}	Ω	24	18	29
Q (CPE_{porous})	Ss^ncm^{-2}	-	1.14×10^{-3}	1.95×10^{-5}	Q (CPE_{porous})	Ss^ncm^{-2}	-	1.50×10^{-4}	1.77×10^{-4}
n_{porous}		-	0.45	0.5	n_{porous}		-	0.50	0.51
R_{Porous}	Ωcm^2	-	31	57	R_{Porous}	Ωcm^2	-	8	45
Q (CPE_{Oxide})	Ss^ncm^{-2}	8.67×10^{-5}	1.72×10^{-4}	2.85×10^{-5}	Q (CPE_{Oxide})	Ss^ncm^{-2}	4.84×10^{-5}	7.91×10^{-5}	1.05×10^{-5}
n_{oxide}		0.9	0.80	0.88	n_{oxide}		0.89	0.79	0.92
R_{oxide}	Ωcm^2	2192	6875	60 493	R_{oxide}	Ωcm^2	2654	9021	49 841
Q (CPE_{dl})	Ss^ncm^{-2}	2.03×10^{-3}	6.92×10^{-4}	1.31×10^{-4}	Q (CPE_{dl})	Ss^ncm^{-2}	1.03×10^{-3}	3.19×10^{-4}	7.74×10^{-5}
n_{dl}		0.77	0.74	0.7	n_{dl}		0.6	0.75	0.83
R_{pol}	Ωcm^2	4201	7574	62 693	R_{pol}	Ωcm^2	6144	15 948	29 750
χ^2		2.5×10^{-4}	2.8×10^{-4}	1.1×10^{-3}	χ^2		1.8×10^{-3}	1.5×10^{-4}	5.0×10^{-4}
AA5083					**AA6014**				
EC		Unexposed 1	Without inhibitor 1	Lithium-leaching 3	EC		Unexposed 1	Without inhibitor 2	Lithium-leaching 3
R_{sol}	Ω	17	19	26	R_{sol}	Ω	21	22	13
Q (CPE_{porous})	Ss^ncm^{-2}	-	-	2.73×10^{-4}	Q (CPE_{porous})	Ss^ncm^{-2}	-	2.46×10^{-5}	2.2×10^{-4}
n_{porous}		-	-	0.5	n_{porous}		-	0.69	0.81
R_{Porous}	Ωcm^2	-	-	18	R_{Porous}	Ωcm^2	-	21	35
Q (CPE_{Oxide})	Ss^ncm^{-2}	1.51×10^{-5}	1.67×10^{-5}	5.11×10^{-6}	Q (CPE_{Oxide})	Ss^ncm^{-2}	1.40×10^{-5}	9.36×10^{-6}	1.27×10^{-5}
n_{oxide}		0.86	0.83	0.93	n_{oxide}		0.88	0.88	0.88
R_{oxide}	Ωcm^2	15 000	156 190	500 000	R_{oxide}	Ωcm^2	10 174	77 722	146 490
Q (CPE_{dl})	Ss^ncm^{-2}	6.90×10^{-4}	9.04×10^{-5}	9.02×10^{-7}	Q (CPE_{dl})	Ss^ncm^{-2}	6.18×10^{-4}	2.63×10^{-5}	3.59×10^{-5}
n_{dl}		0.69	0.82	0.89	n_{dl}		0.88	0.71	0.76
R_{pol}	Ωcm^2	9863	160 170	1 690 200	R_{pol}	Ωcm^2	5780	431 000	474 670
χ^2		2.03×10^{-3}	3.29×10^{-3}	6.7×10^{-4}	χ^2		3.46×10^{-3}	8.25×10^{-4}	3.01×10^{-3}

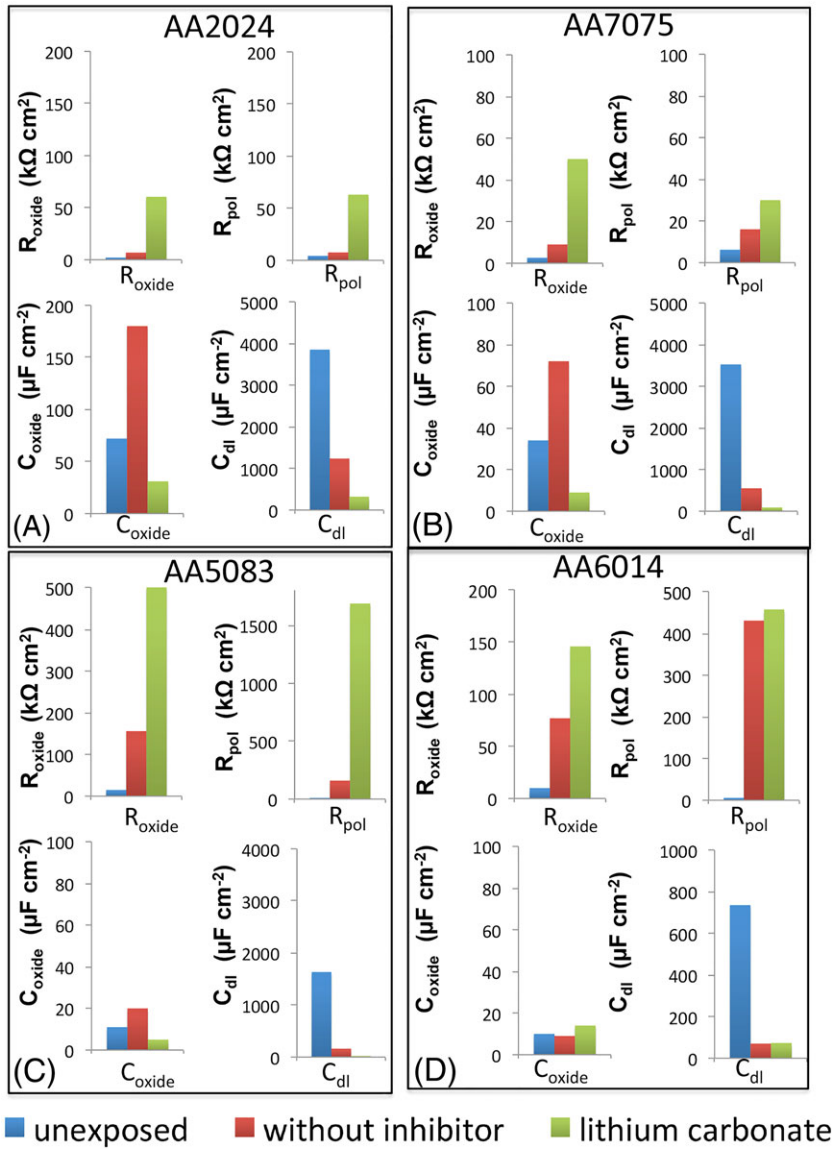

FIGURE 8 Comparison of the electrochemical parameters, oxide resistance (Roxide), polarisation resistance (Rpol), oxide capacitance (Coxide), and double layer capacitance (cdl) in the defect areas of the different alloys coated with coatings with and with Li-carbonate before and after NSS exposure: A, AA2024; B, AA7075; C, AA5083; and D, AA6014

loaded coating provides effective corrosion inhibition on AA7075 and AA5083 as well.

Aluminium alloy AA6014 (Figure 8D) exhibits a different behaviour compared with the other alloys. The unexposed AA6014 sample shows a low R_{oxide} (10 kΩ.cm^2) and R_{pol} (6 kΩ.cm^2) and a high C_{dl} (735 µF/cm^2) which indicates susceptibility to corrosion. However, the alloy shows significantly increased R_{oxide} and R_{pol} values of, respectively, 70 kΩ.cm^2 and 440 Ω.cm^2 for both samples AA6014WO and AA6014W after the NSS exposure. The cross-sectional analysis of AA6014W showed the formation of a protective layer in the defect area when the sample was exposed to NSS. The layer provides a R_{oxide} of 145 kΩ.cm^2, which is double of the R_{oxide} of the sample AA6014WO. The polarisation resistance (R_{pol}) of the exposed samples increased dramatically compared with the unexposed sample to values of approximately 450 kΩ.cm^2, and the double layer capacitance (C_{dl}) of the samples dropped to 70 µF/cm^2 which indicates improved corrosion protection. These results imply that AA6014 has a kind self-passivating property after initial corrosion phenomena, and the protective layer generated in the defect area of the AA6014W sample provides additional corrosion protection without local corrosion phenomena at the alloy surface.

3.5 | Active corrosion protection of different alloys with Li-leaching coatings

Fast and effective corrosion inhibition is an essential requirement for active protective coatings. Especially, for the protection of aluminium alloys that are carefully engineered to fulfil specific industrial requirements by alloying and tempering. The electrochemical properties or corrosion susceptibility of an aluminium alloy are determined by the type, concentration, and distribution of intermetallic or second phase particles in the matrix and the temper. Addition of alloying metals such

as copper, magnesium, silicon, and zinc to the aluminium influences the mechanical properties of the aluminium alloy and also changes the electrochemical behaviour of the alloys as well. For example, the addition of copper and silicon shifts the corrosion potential of an alloy to more noble corrosion potentials increasing cathodic reaction kinetics.[13] The alloys studied in this work were selected because of their inherent different electrochemical activity. AA2024-T3 (Al-Cu-(Mg)) and AA7075-T6 (Al-Zn-Mg (Cu)) were selected as alloys with a high corrosion susceptibility and AA5083-H111(Al-Mg-(Mn)) and AA6014-T4 (Al-Mg-Si-(Cu)) for their low corrosion susceptibility.[30] The intrinsic corrosion susceptibility of these alloys was confirmed by electrochemical means and the microscopy evaluation. There are many corrosion tests available to evaluate the corrosion resistance of aluminium alloys. Amongst them, continuous NSS, cyclic salt spray acidified, or copper-assisted salt spray methods using a wide range of concentrations and electrolytes. The selection of the corrosion test depends on the application and industry. In this work, the coated aluminium samples were exposed to continuous salt spray conditions using the NSS accelerated corrosion test according to ASTM B-117 to compare the active corrosion protection of the Li-leaching coatings on other alloys than AA2024-T3 under equivalent test conditions. All aluminium alloys coated with the coating without Li-carbonate showed local corrosion phenomena due to their microstructure and second phase particles.[4,13,31,32] As expected, both the high strength aluminium alloys, AA2024-T3 and AA7075-T6, showed significantly more corrosion in the defect area compared with the other alloys. However, the "corrosion-resistant" aluminium alloys AA6014-T4 and AA5083-H111 were not free of localized corrosion either.

In contrast to this, the lithium-leaching coatings were able to suppress these localized corrosion phenomena by the formation of a protective aluminium oxide/hydroxide layer as a result of the competitive growth-dissolution reaction at the aluminium/solution interface under alkaline conditions (pH 9-10).[11] A similar protective layer was formed on the aluminium substrate in the defect areas providing additional corrosion protection for all aluminium alloys, independent of their different electrochemical activity. The layer thickness and morphology of the protective layer were similar for all alloys, but the magnitude of the resulting electrochemical properties are different. The corrosion inhibiting effect of the lithium-leaching coatings seems to be more pronounced on the alloys with relatively large amounts of alloying constituents and higher electrochemical activity (corrosion susceptibility), AA2024-T3 (4%-5% Cu), AA7075-T6 (5%-6% Zn and 1%-2% Cu), and AA5083-H111 (4%-5% Mg). The corrosion inhibiting effect on AA6014 seems relatively small between the samples with Li-carbonate and no inhibitor after NSS exposure; this implies a certain self-passivating property of the AA6014-T4 alloy when exposed to a corrosive environment.

The work in this paper shows that all the studied aluminium alloys can be affected by (local) corrosion phenomena when the coating is damaged and the substrate is exposed to a corrosive environment such as the NSS corrosion test. Therefore, it is essential that the active corrosion protection mechanism provides a fast and effective protection by the formation of an irreversible layer on the exposed substrate in the defect which will act as a new barrier to prevent further corrosion. It demonstrated that the active protective nature of the Li-carbonate leaching coatings is not limited to AA2024-T3 and that it is possible to effectively protect the defect areas from local corrosion effects by the generation of a corrosion protective layer in the defect areas of AA7075-T6, AA5083-H111, and AA6014-T4 samples after 168-hour NSS exposure by using a Li-carbonate loaded coating for active corrosion protection. Such an active protective behaviour independent of the metallurgy of the aluminium alloy has not been demonstrated by any other chromate-free corrosion inhibitor. These results demonstrate that Li-salts can be considered as a promising and new class of environmentally-friendly corrosion inhibitors for the protection of a wide range of aluminium alloys even for applications outside the aerospace industry.

4 | CONCLUSIONS

The active protective properties of the lithium-leaching coatings on different aluminium alloys were investigated using scanning electron microscopy and electrochemical techniques. Li-carbonate leaching coatings provided effective corrosion inhibition on a range of aluminium alloys independent of their metallurgy and electrochemical activity. The largest corrosion inhibiting effects were observed on high strength aluminium alloys, AA2024-T3, AA7075-T6, which are known for their active and corrosion susceptible behaviour. The lithium-leaching coatings also suppressed localized corrosion and provided additional corrosion resistance on more corrosion resistant aluminium alloys such as AA5083-H111 and AA6014-T4. Planar view and cross-sectional SEM-analysis revealed that the characteristic three-layered protective layer was generated with a similar thickness and morphology on all investigated alloys. Complementary EIS measurements demonstrated the corrosion protective properties of the generated layer in the defect area of the different alloys. Further analysis of the EIS data enabled the quantification of electrochemical properties associated with the protective layer on the different aluminium alloys.

ACKNOWLEDGEMENTS

The authors would like to acknowledge Wilma Ravesloot of AkzoNobel Specialty Chemicals for their assistance preparing the ion-milled cross sections and Marc Raes for his assistance with the FE-SEM analysis This research was carried out under the collaboration agreement between AkzoNobel and Delft University of Technology.

ORCID

Peter Visser https://orcid.org/0000-0002-6388-382X

REFERENCES

1. Buchheit RG. A compilation of corrosion potentials reported for intermetallic phases in aluminum alloys. *J Electrochem Soc*. 1995;142(11):3994.
2. Birbilis N, Buchheit RG. Electrochemical characteristics of intermetallic phases in aluminum alloys. *J Electrochem Soc*. 2005;152(4):B140.

3. Szklarska-Smialowska Z. Pitting corrosion of aluminum. *Corros Sci*. 1999;41(9):1743-1767.
4. Yasakau KA, Zheludkevich ML, Lamaka SV, Ferreira MGS. Role of intermetallic phases in localized corrosion of AA5083. *Electrochim Acta*. 2007;52(27):7651-7659.
5. Gui J, Devine TM. Influence of lithium on the corrosion of aluminum. *Scri Metall*. 1987;21(6):853-857.
6. Buchheit RG, Bode MD, Stoner GE. Corrosion-resistant, chromate-free talc coatings for aluminum. *Corrosion*. 1994;50(3):205-214.
7. Visser P, Liu Y, Terryn H, Mol JMC. Lithium salts as leachable corrosion inhibitors and potential replacement for hexavalent chromium in organic coatings for the protection of aluminum alloys. *J Coat Technol Res*. 2016;13(4):557-566.
8. Gharbi O, Thomas S, Smith C, Birbilis N. Chromate replacement: what does the future hold? *NPJ Mater Degrad*. 2018;2(1):12.
9. Visser P, Liu Y, Zhou X, et al. The corrosion protection of AA2024-T3 aluminium alloy by leaching of lithium-containing salts from organic coatings. *Faraday Discuss*. 2015;180:511-526.
10. Visser P, Lutz A, Mol JMC, Terryn H. Study of the formation of a protective layer in a defect from lithium-leaching organic coatings. *Prog Org Coat*. 2016;99:80-90.
11. Visser P, Gonzalez-Garcia Y, Mol JMC, Terryn H. Mechanism of passive layer formation on AA2024-T3 from alkaline lithium carbonate solutions in the presence of sodium chloride. *J Electrochem Soc*. 2018;165(2):C60-C70.
12. Visser P, Meeusen M, Gonzalez-Garcia Y, Terryn H, Mol JMC. Electrochemical evaluation of corrosion inhibiting layers formed in a defect from lithium-leaching organic coatings. *J Electrochem Soc*. 2017;164(7):C396-C406.
13. Liang WJ, Rometsch PA, Cao LF, Birbilis N. General aspects related to the corrosion of 6xxx series aluminium alloys: exploring the influence of Mg/Si ratio and Cu. *Corros Sci*. 2013;76:119-128.
14. T. A. A. Inc. *International Alloy Designations and Chemical Composition Limits for Wrought Aluminum and Wrought Aluminum Alloys*. Arlington, VA, USA: The Aluminum Association Inc.; 2015.
15. Stern M, Geary AL. Electrochemical Polarization. *J Electrochem Soc*. 1957;104(1):56.
16. Zawodzinski TA. *Electrochemical Society Interface*. 2009;59.
17. Mata D, Serdechnova M, Mohedano M, et al. Hierarchically organized Li–Al-LDH nano-flakes: a low-temperature approach to seal porous anodic oxide on aluminum alloys. *RSC Adv*. 2017;7(56):35357-35367.
18. Zhang Y, Liu J, Li Y, Yu M, Li S, Xue B. Fabrication of inhibitor anion-intercalated layered double hydroxide host films on aluminum alloy 2024 and their anticorrosion properties. *J Coat Technol Res*. 2015;12(2):293-302.
19. Liu Y, Visser P, Zhou X, et al. Protective film formation on AA2024-T3 aluminum alloy by leaching of lithium carbonate from an organic coating. *J Electrochem Soc*. 2016;163(3):C45-C53.
20. F.C. Campbell, Chapter 26 Aluminium in: Elements of metallurgy and engineering alloys, (2008) 488-508.
21. Ilevbare GO, Scully JR. Mass-transport-limited oxygen reduction reaction on AA2024-T3 and selected intermetallic compounds in chromate-containing solutions. *Corrosion*. 2001;57(2):134-152.
22. Xu DK, Birbilis N, Rometsch PA. The effect of pre-ageing temperature and retrogression heating rate on the strength and corrosion behaviour of AA7150. *Corros Sci*. 2012;54:17-25.
23. Van der Linden B, Terryn H, Vereecken J. Investigation of anodic aluminium oxide layers by electrochemical impedance spectroscopy. *J Appl Electrochem*. 1990;20(5):798-803.
24. Tedim J, Zheludkevich ML, Bastos AC, Salak AN, Lisenkov AD, Ferreira MGS. Influence of preparation conditions of layered double hydroxide conversion films on corrosion protection. *Electrochim Acta*. 2014;117:164-171.
25. Zheludkevich ML, Yasakau KA, Poznyak SK, Ferreira MGS. Triazole and thiazole derivatives as corrosion inhibitors for AA2024 aluminium alloy. *Corros Sci*. 2005;47(12):3368-3383.
26. Hsu CH, Mansfeld F. Technical note: Concerning the conversion of the constant phase element parameter Y0 into a capacitance. *Corrosion*. 2001;57(9):747-748.
27. Liu Y, Visser P, Zhou X, et al. An investigation of the corrosion inhibitive layers generated from lithium oxalate-containing organic coating on AA2024-T3 aluminium alloy. *Surf Interface Anal*. 2016;48(8):798-803.
28. Hirschorn B, Orazem ME, Tribollet B, Vivier V, Frateur I, Musiani M. Determination of effective capacitance and film thickness from constant-phase-element parameters. *Electrochim Acta*. 2010;55(21):6218-6227.
29. Amor YB, Sutter EMM, Takenouti H, Orazem ME, Tribollet B. Interpretation of electrochemical impedance for corrosion of a coated silver film in terms of a pore-in-pore model. *J Electrochem Soc*. 2014;161(14):C573-C579.
30. Davis JR. Corrosion of aluminum and aluminum alloys, ASM International; 1999.
31. Buchheit RG, Grant RP, Hlava PF, McKenzie B, Zender GL. Local dissolution phenomena associated with S phase (Al[sub 2]CuMg) particles in aluminum alloy 2024-T3. *J Electrochem Soc*. 1997;144(8):2621.
32. Andreatta F, Terryn H, De Wit JHW. Corrosion behaviour of different tempers of AA7075 aluminium alloy. *Electrochim Acta*. 2004;49(17-18):2851-2862.
33. Kaufman JG. In Introduction to aluminum alloys and tempers, ASM International, 2000: 87.

How to cite this article: Visser P, Terryn H, Mol JMC. Active corrosion protection of various aluminium alloys by lithium-leaching coatings. *Surf Interface Anal*. 2019;1–12. https://doi.org/10.1002/sia.6638